4914–4924 *Nucleic Acids Research, 2012, Vol. 40, No. 11* *Published online 22 February 2012*
doi:10.1093/nar/gks176

Post-transcriptional homeostasis and regulation of MCM2–7 in mammalian cells

Chen-Hua Chuang[1], Dian Yang[1], Gongshi Bai[1], Amy Freeland[2], Steven C. Pruitt[2] and John C. Schimenti[1,*]

[1]Department of Biomedical Sciences and Center for Vertebrate Genomics, Cornell University College of Veterinary Medicine, Ithaca, NY 14853 and [2]Department of Molecular and Cellular Biology, Roswell Park Cancer Institute, Buffalo, NY 14263, USA

Received September 14, 2011; Revised February 2, 2012; Accepted February 4, 2012

ABSTRACT

The MiniChromosome Maintenance 2-7 (MCM2-7) complex provides essential replicative helicase function. Insufficient MCMs impair the cell cycle and cause genomic instability (GIN), leading to cancer and developmental defects in mice. Remarkably, depletion or mutation of one Mcm can decrease all Mcm levels. Here, we use mice and cells bearing a GIN-causing hypomophic allele of *Mcm4* (*Chaos3*), in conjunction with disruption alleles of other Mcms, to reveal two new mechanisms that regulate MCM protein levels and pre-RC formation. First, the *Mcm4*^{Chaos3} allele, which disrupts MCM4:MCM6 interaction, triggers a *Dicer1* and *Drosha*-dependent ~40% reduction in *Mcm2–7* mRNAs. The decreases in Mcm mRNAs coincide with up-regulation of the miR-34 family of microRNAs, which is known to be *Trp53*-regulated and target Mcms. Second, MCM3 acts as a negative regulator of the MCM2–7 helicase *in vivo* by complexing with MCM5 in a manner dependent upon a nuclear-export signal-like domain, blocking the recruitment of MCMs onto chromatin. Therefore, the stoichiometry of MCM components and their localization is controlled post-transcriptionally at both the mRNA and protein levels. Alterations to these pathways cause significant defects in cell growth reflected by disease phenotypes in mice.

INTRODUCTION

In eukaryotes, the amount and timing of DNA replication are tightly controlled to conduct a single genome replication during S phase (1). Perturbations of the replication machinery can alter ploidy, genome stability and the cell cycle. In late mitosis to early G1, replication machinery assembles at numerous locations (replication 'origins') in the genome to form a pre-replicative complex (pre-RC). The process begins with binding of the Origin Recognition Complex (ORC) to origins, followed by CDC6 and CDT1 which load the MCM2–7 replicative helicase, then other factors needed for helicase activity and competence ('licensing') to initiate DNA replication (1). Although cells contain far more MCM2–7 protein than is required to complete DNA replication, excess chromatin-bound MCM2–7 complexes occupy dormant or 'backup' origins that can be activated to complete DNA replication near stalled or disrupted primary replication forks (2–4). Humans with mutations in any of several pre-RC components are afflicted with a severe developmental syndrome known as Meier-Gorlin (5–7). Mice with decreased (40% or more) MCM levels are susceptible to genomic instability (GIN), cancers and developmental defects (8–10) due to fewer backup origins (11).

While these studies demonstrate that proper homeostasis of the DNA-licensing process is critical for health, little is known about the regulation of these factors in mammals. However, multiple studies in cultured cells and mice reported a phenomenon whereby genetic- or siRNA-induced depletion of a single MCM causes depletion of the other MCMs (3,4,8,9,11–14). It was generally assumed that the pan-decreases were due to MCM2–7 hexamer destabilization. However, single MCM knockdown in *Drosophila*, induced MCM2–7 instability in human cultured cells, and a hypomorphic allele of the mouse *Mcm4* (*Mcm4*^{Chaos3}) all showed an mRNA pan-down-regulation coordinate with decreased protein levels (10,15,16). The underlying mechanism is unknown.

DNA replication can also be regulated at the level of pre-RC component loading. Studies in yeast indicate that all six MCMs (MCM2–7) can load onto replication origins as a ring-shaped toroidal heterohexamer, and there is substantial evidence that this constitutes the eukaryotic replicative helicase (17). However, MCM4/6/7 are typically co-isolated during biochemical purifications as a subcomplex, either as trimers or double trimers $(MCM4/6/7)_2$ with *in vitro* helicase activity. Analyses of

*To whom correspondence should be addressed. Tel: +1 607 253 3636; Fax: +1 607 253 3789; Email: jcs92@cornell.edu

purified complexes *in vitro* indicate that MCM4/6/7 are the 'core' helicase (17–20), whereas MCM3/5 dimers provide negative regulatory function (21,22). We previously found that genetic reduction of MCM3 ameliorates numerous mutant phenotypes exhibited by mice and cells depleted for other MCMs, including cancer susceptibility, embryonic lethality and defective cell cycle/proliferation (10). Paradoxically, this rescue by MCM3 depletion occurred by increasing the amounts of chromatin-bound MCM2–7 *in vivo*, and thus may work by modulating loading of pre-RC components.

In this study, we exploit the *Mcm4*^{Chaos3} model to reveal two novel mechanisms for post-transcriptional regulation of replication licensing *in vivo*. One occurs at the mRNA level and is modulated by the small RNA regulatory pathway to trigger pan-down-regulation of all Mcms. This suggests the existence of a novel regulatory relationship for governing the stoichiometry of the MCM DNA-replication licensing complex in response to replication stress or other situations. The other mechanism involves negative regulation of MCM2–7 access to chromatin by a MCM3:MCM5-containing complex. Furthermore, these *in vivo* studies provide insight into the relevance of *in vitro* experiments on the function of MCM complexes in whole organisms.

MATERIALS AND METHODS

Lentiviral expression vectors

Doxycycline inducible lentiviral vectors (23) were prepared by co-transecting viral packaging plasmids psPAX2 and pMD2.G with vectors encoding rtTA, LacZ, *Mcm2, Mcm3, Mcm4* or *Mcm3* mutant into 293T cells using TransIT-Lt1 transfection reagent (Mirus). Viral supernatants were collected at 48 and 72 h and concentrated. Mouse embryonic fibroblasts (MEFs; P1–P3) seeded at 6.75×10^3 cells/cm^2 and incubated for 24 h were infected with lentiviral vectors. After 24 h, 2 μg/ml doxycycline (Sigma) was added, and the cells were cultured for 5 days before flow cytometric analysis (described below). For HeLa cell infection, 1000 cells were seeded into 150 mm tissue culture dishes and cultured for 14 days before infection. Plates were fixed and colonies visualized with Crystal Violet.

Protein and cellular fractionation

A Triton-100 based fractionation of chromatin-bound versus non-chromatin-bound proteins was used. In this protocol, nuclei pelleted from lysed cells contained nuclear scaffold proteins, DNA and chromatin binding forms of MCMs. The supernatant (detergent soluble fraction, referred to in the text as 'soluble' versus the chromatin bound or 'extracted' proteins) contained proteins of the cell membrane, cytosol and free forms of MCMs (4,24). For protein extraction, the nuclear pellet was washed twice with 1 ml TX-NE (320 mM sucrose, 7.5 mM $MgCl_2$, 10 mM HEPES, 1% Triton X-100 and a protease inhibitor cocktail) and resuspended in 0.5 ml RIPA. Successful partitioning was assessed not only with Western blotting controls, but with flow cytometric analysis of detergent-extracted whole nucleus preps (Supplementary Figure S1a), which were consistent with prior studies (25).

MEF culture

Mouse embryonic fibroblasts (MEFs) from 12.5- to 14.5-dpc embryos were cultured in Dulbecco's-Modified Eagle's Medium (DMEM) supplemented with 10% FBS, 2 mM GlutaMAX, penicillin–streptomycin (100 U/ml) and β-mercaptoethanol. All assays were conducted on cells at early passages (up to 2–3 weeks after initial isolation from embryos).

RNA interference

ON-TARGETplus SMARTpool small interfering RNA (siRNA) was purchased from Dharmacon (Lafayette, CO, USA). MEFs were seeded on six-well plates at 1×10^5 cells/well and grown for 12 h. The cells were then transfected with siRNAs against mouse *DicerI* (Mix of GGUAGACUGUGGACCGUUU, GGAAAUACCUGUACAACCA, GCAAUUUGGUGGUUGGUUU and ACAGGAAUCAGGAUAAUUA), *Drosha* (UGGAAGGAGUUACGCUUUA, GCCAAAUACGGAUCGGCAA, UGUGUAAAGUGAUUCGAUU and GGAUGGAAUUUCUGGGCGA), or an unrelated scrambled siRNA (CCUACUAAGCGACACCAUUdTdT) at a final concentration of 100 nM using DharmaFECT1 (Dharmacon). After 24 h, the transfection medium was replaced with DMEM. The cells were harvested 96 or 120 h post-transfection for qRT-PCR analysis.

Micronucleus assays

These were performed essentially as described (26).

Chromatin immunoprecipitation assays

Mouse embryonic fibroblasts (MEFs) were plated at 4×10^6 cells/150 mm culture plate for 60 h, then treated for 10 min at room temperature in 1% formaldehyde to crosslink chromatin proteins to DNA. The reaction was stopped with 0.125 M glycine for 5 min. Cells were pelleted and resuspended in 1 ml sonication buffer (Upstate) for 10 min on ice. About 450 μl were sonicated to generate 500-bp fragments on average (300–700 bp). A total of 100 μg of DNA–chromatin complexes were processed according to the *EZ ChIP*^{TM} (Upstate) kit protocol. Monoclonal anti-RNA polymerase II (phospho S2; Covance) and rabbit anti-mouse IgM antibody (Millipore) were incubated together for immunoprecipitation. DNA was purified by phenol–chloroform extraction and ethanol precipitation.

For quantitative PCR analysis of RNA polymerase II-bound targets, the immunoprecipitated (IP'd) DNA was resuspended in 100 μl of water. Input DNA was used as reference.

Co-immunoprecipitation

Cells (1×10^6) were transfected with an expression plasmid using Lipofectamine 2000 (Invitrogen). After 72 h, total protein was extracted using RIPA buffer (50 mM

Tris–HCl pH 8.0, 150 mM NaCl, 0.1% SDS, 1% NP-40, 1 mM EDTA, 0.5% Sodium Deoxycholate and 50 mM NaF) with protease inhibitor (Protease Inhibitor Cocktail Tablets, Roche Cat. No. 11836153001). After centrifugation (10 000*g* for 10 min), the supernatant was incubated with primary antibody at 4°C overnight and then with Protein A Agarose (Millipore, Cat. No. 16-125) at room temperature for 1 h, followed by three washes in RIPA. Bound proteins were denatured by boiling in sample buffer and used for SDS–PAGE and western blotting.

For detecting ecotopic *Mcm4* variants in HEK cells, anti-FLAG (Sigma F3165) was used. For reciprocal co-IP experiments, anti-MCM6 (Santa Cruz sc-9843) and anti-MCM7 (Cell Signaling #4176) were used.

Western blot analysis

The concentration of protein samples were quantified with a BCA kit (Pierce). Fifteen micrograms of total protein were separated by SDS–PAGE, electrotransferred onto a pure nitrocellulose membrane (Bio-Rad), and probed with the relevant antibodies. Binding was detected with a Pierce ECL kit and autoradiography. For quantifying immunoblotting, ECL bands on the film were scanned (grayscale at 800 dpi), saved as TIFF images, and ImageJ software (http://rsb.info.nih.gov/ij/) was used to create an Integrated Density Value (IDV) for each band. Background correction was done using a 'rolling ball' method with a radius of four times the width of a band.

The antibodies used were as follows: MCM2: ab31159 (Abcam); MCM3: 4012 (Cell Signaling); MCM4: ab4459 (Abcam); MCM5: NB100-78261 (Novus); MCM6: NB100-78262 (Novus); MCM7: ab2360 (Abcam); MYC: Mouse Monoclonal Anti-c- Myc M4439 (Sigma); FLAG: Rabbit Polyclonal Anti-FLAG #2368 (Cell Signaling); Fibrillarin: ab5821 (Abcam) GAPDH: 6C5 (Advanced Immunochemical); and β-actin: A1978 (Sigma).

Luciferase constructs and assays

The promoter regions of *Mcm2*, *Mcm5*, *Mcm7* and *Pgk2* (300-bp upstream of the annotated transcriptional start sites) were PCR amplified from mouse genomic DNA (PCR primers are listed in Supplementary Table S1) and cloned into the pGL4.14 luciferase-containing plasmid (Promega). MEFs were plated at 7.5×10^4 cells/well in 24-well plates. Cells were transfected using FuGENE HD reagent and a total of 850 ng DNA/well consisting of mouse Mcms (2, 5 or 7) and *Pgk2* reporter constructs. Cells were lysed in reporter lysis buffer (Promega) after 24 h, and assayed for luciferase activity. Results were standardized to the *Pgk2*-Luc activity levels.

Quantitative RT-PCR

Mouse embryonic fibroblasts (MEFs) were seeded at 1×10^6 cells/100 mm culture plate for 24 h. For assaying protein-coding genes, total RNA was isolated using Qiagen RNeasy kits. After DNAse I (Invitrogen) treatment, cDNA was synthesized from 1 μg of total RNA using the Invitrogen SuperScript III Reverse Transcriptase kit in a total volume of 20 μl with the supplied Oligo-dT or random-hexamer primers. qPCR reactions were performed in triplicate on 1 ng or 10 ng of cDNA using the SYBR power green RT-PCR Master kit (Perkin Elmer Applied Biosystems; 40 cycles at 95°C for 10 s and at 60°C for 1 min), and real-time detection was performed on an ABI PRISM 7300 (Applied Biosystems) and analyzed with the Geneamp 5700 sds program (PerkinElmer/Applied Biosystems). The specificity of the PCR amplification procedures was checked with a heat-dissociation step (from 60°C to 95°C) at the end of the run and by agarose gel electrophoresis. Results were standardized to β-actin. The PCR primers are listed in Supplementary Table S1.

For qPCR of microRNAs (miRNAs), total RNA preparations that include RNA > 18 nt were purified from MEFs using the miRNeasy Mini Kit (QIAGEN). miRNA quantification was performed using the qScript microRNA Quantification System (Quanta Biosciences). miRNA cDNA was synthesized from 1 μg of RNA using the qScript microRNA cDNA Synthesis Kit (Quanta). qPCR reactions were performed on ABI 7300 PRISM in duplicate using the Power SYBR Green PCR Master Mix (Applied Biosystems; 40 cycles at 95°C for 5 s and at 60°C for 30 s). PerfeCTa microRNA Assay qPCR primers were used (Quanta). The specificity of the qPCR reactions was confirmed with a heat-dissociation step (from 60°C to 95°C) added at the end of the run. Results were standardized to RNU6.

Construction of *Mcm2,3,4* mutants

Mouse DNA fragments were amplified from C3HeB/FeJ cDNA. The $Mcm4^{Chaos3}$ allele was amplified from a mutant homozygote. DNAs were cloned into the pCDNA4-TO-His-Myc express plasmid (Invitrogen) for transient transfection, and pFUW vectors for Lentiviral infection. *Mcm3* mutants were generated by site-directed mutagenesis with the QuikChange kit (Stratagene) according to the manufacturer's instructions. Total sequences were confirmed after finishing the mutagenesis. The primers used in plasmid construction are listed in Supplementary Table S1.

Flow cytometry

For analysis of lentivirus infected cells, $\sim 1 \times 10^6$ MEFs were trypsinized for 10 min, and then washed twice with cold PBS. They were gently but completely resuspended in 1 ml of 4% paraformaldehyde in PBS at room temperature for 30 min. The fixed cells were pelleted by centrifugation at 500*g* for 2 min and washed twice with 10 ml TBS-TX (0.1% Triton X-100) buffer. For antibody staining, the cells were blocked with 1 ml TBS-TX buffer with 1% BSA for 15 min at room temperature, stained with anti-Myc antibodies for 60 min, washed twice and then secondary antibody goat anti-mouse IgG-FITC (South Biotech) with Hoechst 33258 DNA dye, which was applied for 60 min. Immunolabeled cells were analyzed with a 488 nm laser. Cells were considered to be virus-infected if they were FITC positive. Only FITC positive cells were used for cell cycle profiling as determined by Hoechst 33258 staining of DNA content. Calibration of the flow cytometer and gates were set using

uninfected MEFs as negative controls. For flow cytometry of detergent-extracted nuclei, they were resuspended in 50 µl TX-NE, fixed by adding 1 ml 4% PFA for 30 min on ice, pelleted at 500*g* for 2 min, then washed twice with 10 ml TBS-TX (0.1% TX-100) before staining with DAPI, 30′ RNAse treatment (batches optimized empirically) and antibody binding.

hnRNA analysis

This approach for measuring levels of primary (pre-spliced) transcripts has been described (27,28).

RESULTS

Mcm RNA levels are regulated post-transcriptionally

The mouse *Mcm4*^{Chaos3} allele (abbreviated 'C3') causes GIN and cancer in homozygotes (8,11). *Mcm4*$^{C3/C3}$ MEFs have a ~40% reduction in Mcm2–7 mRNA (Figure 1A and B) and protein (10,11), leading to a decrease in dormant origins (10,11). One possible explanation is differential transcription linked to altered cell cycle in mutants. However, cell cycle profiles of *Mcm4*$^{C3/C3}$ ('Chaos3') cultures have minor differences relative to WT (10), and qRT-PCR analysis of numerous cell-cycle regulated genes revealed only minimal (<14%) alterations of the G1/S and S gene mRNA levels (Figure 1A and B). *Cdc6* mRNA was 24% lower (Figure 1B), but this appears to be unrelated to the Mcm2–7 declines; when cell cycle alterations were rescued by *Mcm3* reduction as previously described (10), *cdc6* mRNA levels but not *Mcm2,4-7* mRNA levels were restored (Figure 1C). Additionally, there was no evidence for involvement of the E2F transcription factor family in down-regulating Mcm2–7 transcription in Chaos3 cells, since neither the E2F family nor key downstream targets of E2F (*Pcna*, *Dhfr* and *Ccne1/2*) were down-regulated at all or nearly as much as *Mcm2–7* (Figure 1B).

Four orthogonal experiments showed that the *Mcm2–7* mRNA pan-reduction occurs post-transcriptionally. First, *Mcm2–7* heterogeneous nuclear RNAs (hnRNA; pre-spliced transcripts) were at WT levels in Chaos3 MEFs (Figure 1D). Second, luciferase reporters driven *Mcm2*, *Mcm5* and *Mcm7* promoters in WT and Chaos3 MEFs had no significant activity differences (Figure 1E). Third, transcript levels of the gene trapped *Mcm2*^{Gt} and *Mcm3*^{Gt} alleles were not decreased in Chaos3 versus WT MEFs; in fact, the levels were actually slightly higher in mutant cells (Figure 1F). Fourth, polymerase II occupancy within Mcm transcriptional units in Chaos3 cells was similar to, or higher than, that in WT cells (Figure 1G).

Mcm mRNA levels are affected by RNAi machinery, and their decreases correlate with elevated *miR-34a-c*

To determine if endogenous RNAi pathways control MCM mRNA levels, siRNA-mediated depletions of *Dicer1* and *Drosha* were performed in Chaos3 and control MEFs. *Dicer1* knockdown (68%) in Chaos3 MEFs was accompanied by increase in *Mcm2, 3, 4, 5 and 7* by up to 1.6-fold (Figure 2A). *Drosha* knockdown (72%) caused 1.3- to 1.7-fold increases of Mcm RNAs. No changes were induced by *Dicer* or *Drosha* knockdown in WT cells. These data are consistent with the possibility that endogenous small RNA-mediated degradation mechanisms are responsible for Mcm mRNA depletion in Chaos3 cells. Interestingly, *Dicer* mRNA itself also increased upon *Drosha* knockdown (Figure 2A), suggesting a regulatory relationship as observed by others (29).

miRNAs are an important mechanism of post-transcriptional modulation of gene expression, and the following recent reports led us to suspect that miRNAs may underlie the post-transcriptional down-regulation of Mcms. First, conditional over-expression of miR-34a is associated with decreased MCM2–7 protein and RNA levels (30–32). Second, *Mcm2* and *Mcm5* mRNAs are direct targets of miR-34a in the context of the RISC complex (31). Third, the tumor suppressor TRP53, which transcriptionally activates miR-34a-c (32), is constitutively activated in Chaos3 MEFs and MCM levels increase when *Trp53* is deleted from Chaos3 cells (11).

To determine whether the miR-34 family might be involved in post-transcriptional pan-down-regulation of MCMs in Chaos3 MEFs, their levels were measured by qRT-PCR. In Figure 2B, the levels of miR-34a, miR-34b and miR-34c were increased by 145, 212 and 210%, respectively. Meanwhile, the levels of three miRNAs (miR-25, 93 and 106b) located in an *Mcm7* intron were not increased, consistent with the observation that *Mcm7* transcription is unaffected in Chaos3 MEFs (Figure 1D and E). However, there was a 20% increase in the levels of miR-107, which is known to be up-regulated by TRP53 (33).

The *Mcm4*^{Chaos3} mutation disrupts MCM4:MCM6 interaction

Prior studies, and the data presented here thus far, paint the following scenario to explain genomic instability in *Chaos3* cells: the mutation causes post-transcriptional decreases in Mcm2–7 mRNAs, which in turn decreases MCM2–7 protein levels, leading to a reduction in dormant replication origins. However, it is unclear what initially triggers the reduction of Mcm mRNAs.

The *Mcm4*^{C3} allele encodes a PHE > ILE change at a highly conserved residue (Phe345Ile) that is predicted to reside at the protein–protein interface region of MCM2–7 monomers (34). To explore how this mutation may initiate the aforementioned chain of events, we considered two possibilities. The first is that the *Chaos3* mutation disrupts an intra-hexamer interaction(s) between MCM4 and another MCM(s). The second, based on the finding that MCM2–7 complexes are loaded as double hexamers into pre-RCs (35), is that inter-hexamer interactions are disrupted in a manner that affects the loading or stability of pre-RCs. In either scenario, the cell may sense such defects and respond by down-regulating MCM levels.

To test these possibilities, we determined the ability of MCM4^{C3} to associate with other MCMs in HEK cells, which are efficient for transfection and expression of exogenous constructs. Whereas MCM7 could be co-immunoprecipitated with epitope-tagged mouse

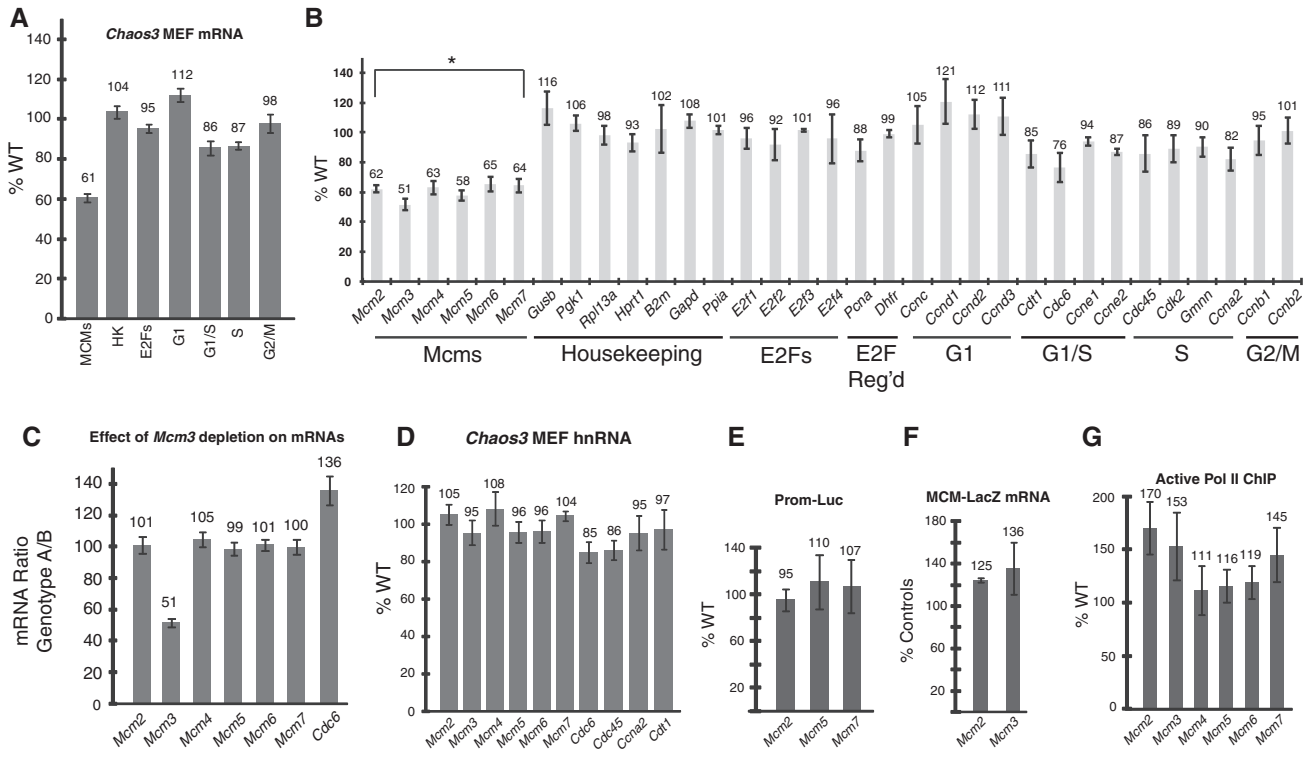

Figure 1. Mcm2–7 mRNAs are reduced post-transcriptionally in $Mcm4^{C3/C3}$ MEFs. (**A**) Combined qRT-PCR analysis of mRNAs from various gene classes: *Mcm2–7* (MCMs); housekeeping (HK); E2F transcription factors (E2Fs); and genes involved in the indicated cell cycle stages. Individual values for each gene within a class are shown in 'B'. Error bars are SEM. (**B**) Relative levels of the indicated mRNAs in $Mcm4^{C3/C3}$ versus WT MEFs. These are the primary data summarized in 'A'. Genes are classified as indicated underneath the graph. Relative transcript levels were normalized to β-actin. $N = 3$ replicate cultures per genotype. (**C**) Hemizygosity for *Mcm3* does not affect the levels of other Mcm mRNAs aside from *Mcm3* itself, but does increase the G1/S-expressed *Cdc6* mRNA due to rescue of cell growth defects (increased G2/M and decreased G1 populations) Genotype A = $Mcm4^{C3/C3}$ $Mcm2^{Gt/+}$ $Mcm3^{Gt/+}$; B = $Mcm4^{C3/C3}$ $Mcm2^{Gt/+}$. (**D**) Mcm2–7 hnRNA levels in $Mcm4^{C3/C3}$ MEFs are unchanged compared to WT. Plotted are qRT-PCR data (% WT) from intron/exon amplimers (primers listed in SI Table 1). $N = 3$ replicates; SEM bars are shown. (**E**) Mcm promoter activity is unchanged in $Mcm4^{C3/C3}$ cells. Plotted are luciferase activities in $Mcm4^{C3/C3}$ MEFs transfected with the indicated promoter-luciferase (Prom-Luc) expression constructs (see 'Materials and Methods' section), with the values relative to transfections into WT MEFs. $N = 5$ replicates; SEM bars are shown. (**F**) mRNA levels of *Mcm2* and *Mcm3* gene trap alleles in $Mcm4^{C3/C3}$ $Mcm2^{GT/+}$ and $Mcm4^{C3/C3}$ $Mcm3^{GT/+}$ MEFs, respectively, are not decreased compared to levels in 'Controls': $Mcm2^{GT/+}$ and $Mcm3^{GT/+}$ MEFs, respectively. The values are produced from qRT-PCR analysis of amplimers representing Mcm-LacZ hybrid transcripts. $N = 3$ replicates; SEM bars are shown. (**G**) ChIP-qPCR analysis of RNA Pol II occupancy within the *Mcm2–7* transcription units of $Mcm4^{C3/C3}$ MEFs. Values are relative to WT, as indicated. $N = 4$ replicates; SEM bars are shown.

$MCM4^{+}$ or $MCM4^{C3}$, MCM6 was only pulled down with $MCM4^{+}$ (Figure 3A). Little or no MCM2, 3 or 5 was co-IP'd with $MCM4^{+}$ or $MCM4^{C3}$ (not shown). Similar results were obtained with endogenous proteins in $Mcm4^{C3/C3}$ MEFs (Figure 3B). Additionally, although anti-MCM6 IP'd MCM7 in WT cells, it did not in *Chaos3* cells (Figure 3B). The disrupted MCM4/6 interaction likely causes MCM2–7 to break into subcomplexes (Figure 3C), as was also suggested by gel filtration studies (11), and our observations of relatively weaker interactions between MCM3 and MCM7 compared to MCM3 and MCM5 (Figure 4F). Since $MCM4^{+}$ and $MCM4^{C3}$co-IP'd each other, this suggests that the mutation does not abolish interactions between MCM2–7 hexamers.

Given the known relationship among MCM2–7 monomers in the intact hexamer (Figure 3B) and the disrupted MCM4/6 interaction in $Mcm4^{C3/C3}$ cells, we surmised that the already reduced $MCM4^{C3}$–MCM7 interaction becomes critical for hexamer stability, since this link is the only one left tethering MCM4 to the rest of the MCM2–7 complex. Consistent with this, *Mcm7* heterozygosity cause a dramatic increase of micronuclei (a metric of GIN) in $Mcm4^{C3}$/+ mice that was even higher than in $Mcm4^{C3/C3}$ cells and all other MCM depletion models (Figure 3D) (10). Notably, the genotype $Mcm4^{C3/C3}$ $Mcm7^{Gt/+}$ causes 97% pre-wean lethality, which is higher than all other combinations tested excepting homozygous nulls (10).

Rescue of MCM depletion phenotypes by genetic reduction of MCM3 is not unique to the *Chaos3* model

We previously reported the paradoxical finding that numerous phenotypes of *Chaos3* mice, the cells of which contained ~40% reduced MCM2–7 levels, were rescued or ameliorated by further genetic reduction of MCM3 (10). These phenotypic rescues by *Mcm3* heterozygosity

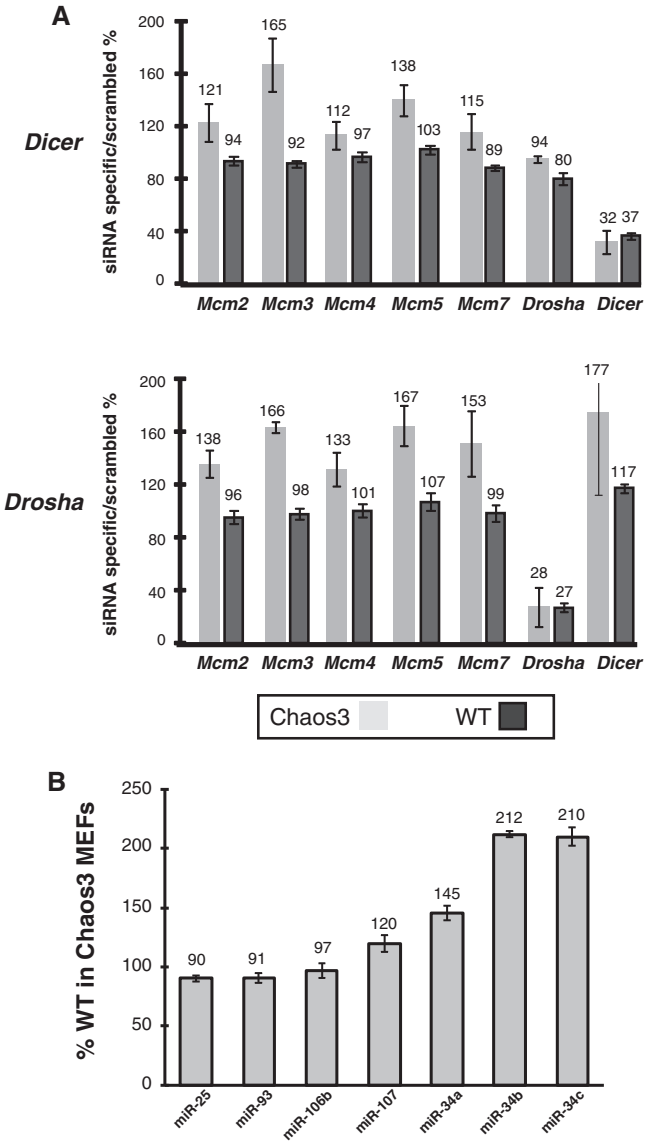

Figure 2. Depletion of Mcm2–7 mRNAs in $Mcm4^{C3/C3}$ cells is *Dicer1* and *Drosha*-regulated, and associated with up-regulation of micro RNAs miR-34a-c. (**A**) The graphs showed qRT-PCR analysis of the indicated genes in $Mcm4^{C3/C3}$ or WT MEFs that were treated with siRNA against *Dicer1* (top) and *Drosha* (bottom) for 120 h. $N = 3$ replicates; SEM bars are shown. Data were standardized against β-actin. (**B**) qRT-PCR analysis of various miRNAs. The values are plotted as percentages of the levels of the indicated miRNAs in $Mcm4^{C3/C3}$ (Chaos3) MEFs versus WT MEFs. The data represent analysis of 5 littermate pairs of MEFs. SEM bars are shown.

included a delay of mammary tumor onset in $Mcm4^{C3/C3}$ females and restored viability of mice bearing the normally lethal $Mcm4^{C3/-}$ genotype. Genetic reductions of MCM2, 6 and 7 in the $Mcm4^{C3/C3}$ background caused additional severe phenotypes (including embryonic lethality, growth defects, anemia and early onset cancer) that were also rescued or diminished by *Mcm3* heterozygosity.

To determine if this phenomenon is unique to or dependent upon the *Chaos3* allele of *Mcm4*, we tested whether MCM3 reduction could rescue the severe phenotypes associated with a different MCM depletion model, $Mcm2^{IRES\text{-}CreERT2}$. Mice homozygous for this allele have 1/3 normal levels of MCM2, exhibit genomic instability, have reduced dormant replication origins, and most die of cancer (primarily lymphoma) at an early age (9,36). Remarkably, *Mcm3* heterozygosity significantly improved the 5 month survival of $Mcm2^{IRES\text{-}CreERT2}$ homozygotes (Table 1). Thus, the phenotype rescue by MCM3 reduction applies to the circumstance of overall MCM2–7 depletion, rather than any specific structural defects in the MCM2–7 helicase caused by the $Mcm4^{Chaos3}$ allele, such as that resulting in the intra-hexamer instability.

MCM3 interaction with MCM5 via a leucine-rich motif correlates with chromatin-bound MCM levels

The rescues of genetic MCM reduction phenotypes by *Mcm3* heterozygosity was associated with increased chromatin-bound MCMs (10), presumably improving pre-RC density that is already decreased in *Chaos3* cells (11). We speculated that this redistribution of the chromatin-depleted MCM pool was attributable to a reduction in MCM3-mediated MCM2–7:XPO1 (exportin 1; the mammalian ortholog of Crm1) interaction, based on the following observations: (i) mammalian MCM3 encodes two predicted leucine-rich potential nuclear export signals (NES) in the same approximate location as a functional NES in yeast Mcm3 (scMcm3) (10,37); (ii) the scMcm3 NES interacts with Crm1 to export Mcms through nuclear pores after DNA synthesis (37); and (iii) MCM interaction with nuclear pore complex (NPC) components regulates binding of MCMs to chromatin and replication licensing in *Xenopus* egg extracts (38,39).

Consistent with this hypothesis, ectopically expressed mouse MCM3 co-IP'd XPO1 in HEK cells (Figure 4A), whereas a mutant version in which three leucines and one isoleucine within the predicted NES were changed to alanines ('L4A'; Figure 4B) abolished MCM3:XPO1 interaction. Over-expression of MCM3 but not $MCM3^{L4A}$ in stably transfected (via lentivirus) HeLa cells, which are known to express very high levels of Mcms (40), caused a decrease of chromatin-bound MCM2, 4, 5, 6 and 7 (Figure 4C; thereby increasing the soluble/chromatin MCM ratio as plotted in Figure 4D) that was not due to an increase of cells arrested in G2/M (Supplementary Figure S1b). Flow cytometric analysis of MCM2 levels in nuclei, which were decreased in G1 cells, were consistent with the Western blot analyses (Supplementary Figure S1a). These changes in MCM2–7 localization had functional correlates with cell growth; over-expression of MCM3 markedly decreased colony formation compared to $MCM3^{L4A}$ (Figure 4C). Since CDK phosphorylation of scMcm3 regulates its nuclear transport ability (37), we also tested whether a presumed phosphorylation-dead version of MCM3 ($MCM3^{S5A}$), in which five predicted MCM3 CDK phosphorylation sites were mutagenized (Figure 4B), lacked the ability to increase MCM2–7 loading and improve cell growth. This was not the case; $MCM3^{S5A}$ transfection had

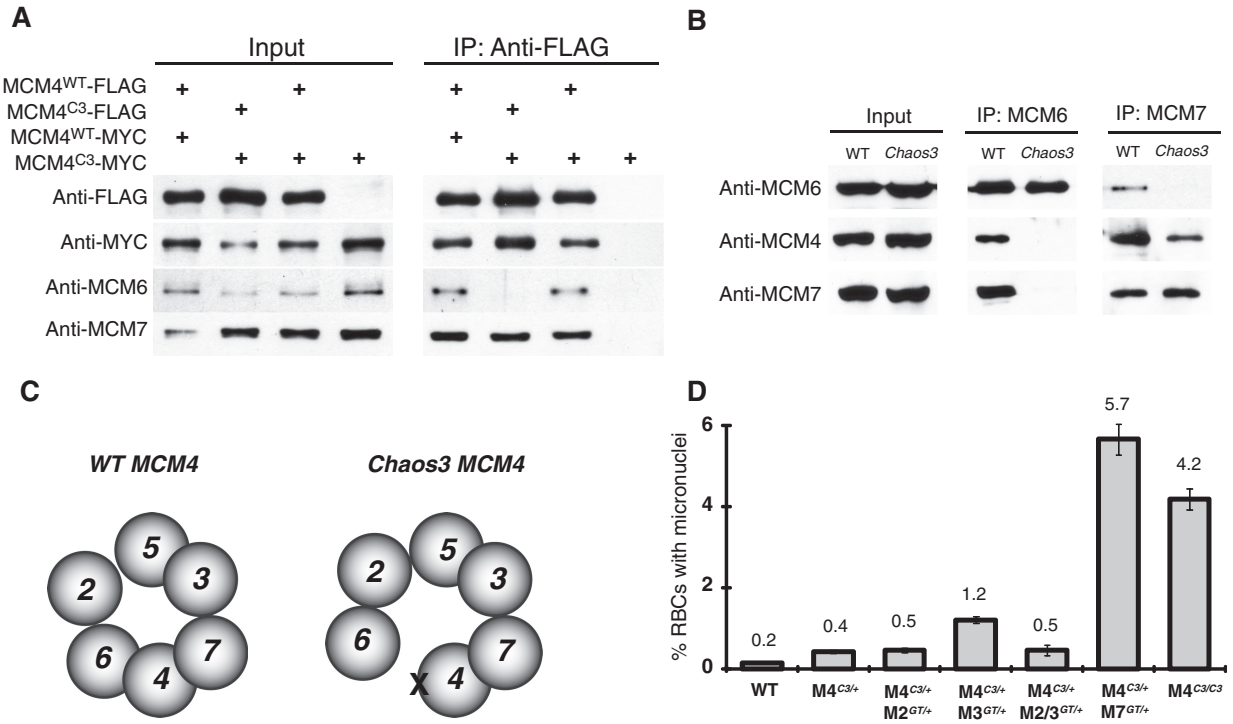

Figure 3. MCM4^{C3} disrupts interaction with MCM6 specifically. (**A**) Western blot analysis of proteins IP'd with ectopically expressed epitope-tagged MCM4 in HEK cells. (**B**) Western blot analysis of proteins IP'd with MCM6 or 7 in the indicated genotypes of immortalized MEFs. Chaos3 = *Mcm4*$^{C3/C3}$. (**C**) Consequence of *Chaos3* mutation on MCM2–7 interactions. 'X' = *Chaos3* mutation. Depicted are known and confirmed interactions of MCM monomers in the MCM2–7 heterohexamer. Strong interactions are depicted as overlaps between monomers (such as MCM4:7), and weaker interactions between monomers are indicated by non-overlapping attachments of the proteins (such as MCM2:6). (**D**) Micronucleus levels in indicated genotypes of male MEFs. 'C3' = *Chaos3*. 'M4' = *Mcm4*. At least five embryos were analyzed for each genotype. SEM bars are shown.

effects similar to the WT construct (Figures 4E, 5A and B). Furthermore, dephosphorylation of protein extracts did not disrupt MCM3:XPO1 interaction (Figure 4A), suggesting that the anti-licensing effects of MCM3 may occur via a mechanism not involving, or in addition to, XPO1 interaction. We posit that the anti-licensing activity of MCM3 might involve interaction of another protein with the leucine-rich domain.

In mammalian cells, MCM3 dimerizes robustly with MCM5 (41,42). It also binds MCM7, but with lower affinity (41). To determine if the leucine-rich motifs in MCM3 mediate these interactions, the abilities of MYC-tagged MCM3 and MCM3^{L4A} to bind these partners were compared in co-IP experiments. As expected, WT MCM3 bound both MCM5 and MCM7, but the L4A mutation completely abolished interaction with MCM5 specifically (Figure 4F). Although CDK-dependent phosphorylation of specific MCM3 S/T sites was reported to stimulate its binding to other MCMs (including MCM5 and MCM7) and loading onto chromatin (41), MCM3^{S5A} maintained strong interactions with MCM5 and MCM7 despite having mutations of these same S/T sites (Figure 4F).

MCM3 modulates cell cycle dynamics by controlling MCM2–7 loading onto chromatin

To investigate MCM3's apparent role as a negative cell cycle regulator, we utilized primary MEFs that exhibit well-characterized phenotypes arising from genetic Mcm depletion. *Chaos3* MEFs, with ~60% WT MCM2–7 levels, exhibit a mild accumulation of G2/M stage cells (8,10). Further genetic reduction of MCM2 to ~17% WT levels (in *Mcm4*$^{C3/C3}$ *Mcm2*$^{Gt/+}$ cells) severely impacted cell growth and viability of mice (10). Cells of this genotype had a 37% increased G2/M population, indicative of cell cycle arrest (Figure 5A). Further genetic reduction of MCM3 (*Mcm4*$^{C3/C3}$ *Mcm2*$^{Gt/+}$ *Mcm3*$^{Gt/+}$), which was shown to partially rescue the poor growth and early senescence of *Mcm4*$^{C3/C3}$ *Mcm2*$^{Gt/+}$ MEFs by increasing MCM binding to chromatin (10), significantly decreased the degree of G2/M arrest (Figure 5A). Mice of this genotype do not suffer the extreme embryonic lethality as do *Mcm4*$^{C3/C3}$ *Mcm2*$^{GT/+}$ animals.

These results predict that increasing MCM3 (above haploinsufficient level) would inhibit cell growth in this model system, but added expression of other MCMs would rescue growth. Indeed, cells expressing ectopic *Mcm2* or *Mcm4* expression rescued the G2/M delay (Figure 5B and C), while expression of WT *Mcm3* (or MCM3^{S5A}) aggravated the G2/M arrest. In contrast, expression of MCM3^{L4A} rescued the G2/M arrest even more efficiently than *Mcm2* or *Mcm4* (Figure 5B), suggesting that this protein improves MCM2–7 function or formation, but that the disrupted interaction with MCM5 and/or XPO1 specifically obliterates the negative regulatory role of MCM3.

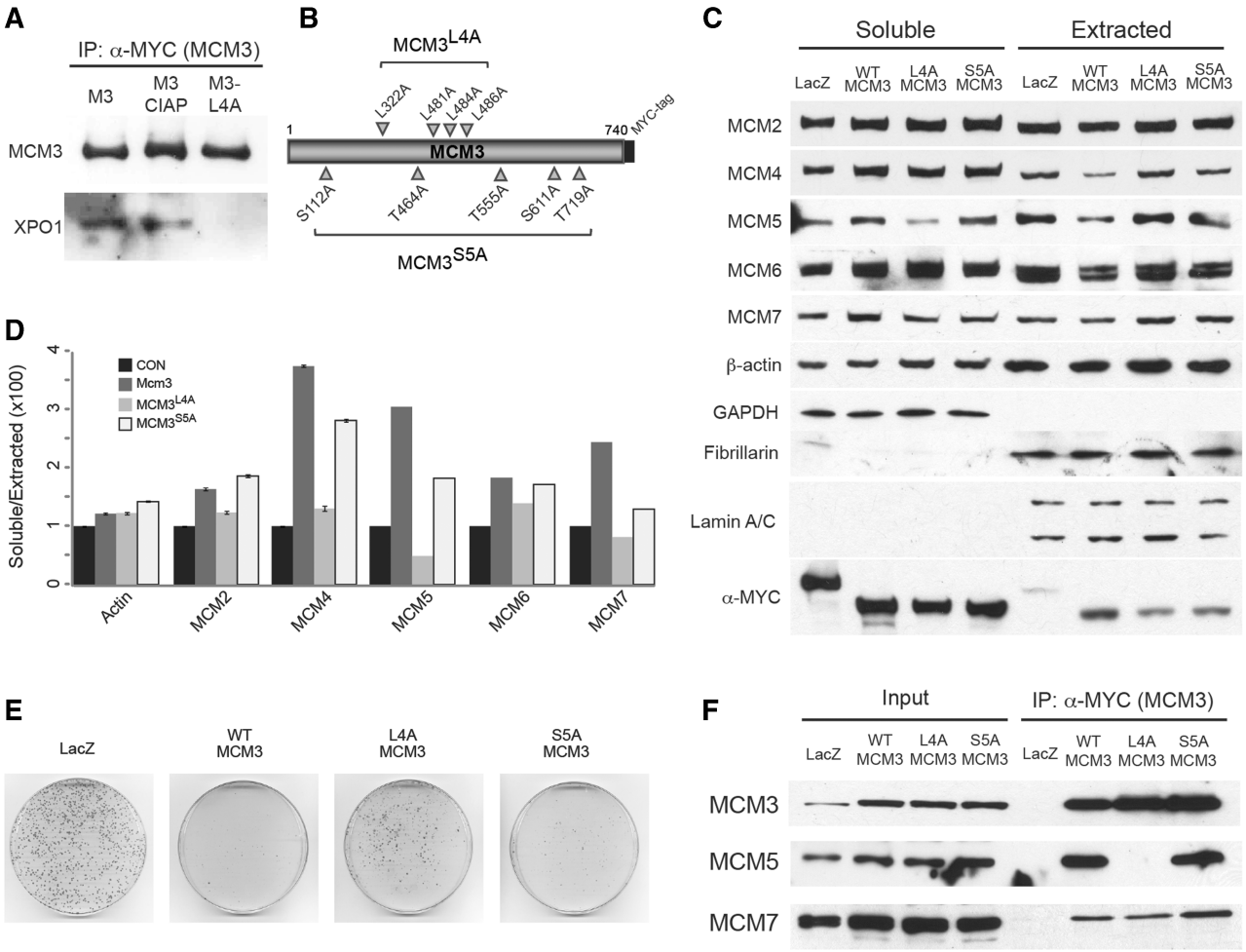

Figure 4. MCM3 interacts with XPO1 and MCM5 via an NES motif that is essential for inhibiting MCM chromatin binding and cell proliferation. (**A**) MCM3 interacts with XPO1 in an NES-dependent manner. Shown are Western blots probed for proteins co-IP'd from HEK cells ectopically expressing MYC tagged mMCM3 (M3) or a version with four Leucines mutated within the putative NES (M3-L4A; see 'B'). The middle lane contains extracts that treated with calf intestinal alkaline phosphatase (CIAP) prior to IP. (**B**) Schematic of mutation made in the putative NES motif (top) and CDK phosphorylation sites (bottom) within MCM3. (**C**) Western blot analysis of the indicated chromatin-bound ('Extracted') and soluble proteins isolated from HeLa cells infected with control (LacZ vector) or MYC-tagged MCM3 lentiviral constructs (listed at top). (**D**) Quantification of Western blot data by densitometry. Intensities of bands in 'A' were normalized against GAPDH in soluble fractions, or fibrillarin in extracted fractions. These values relative to WT cells are plotted. Experiments were repeated twice. (**E**) Images of HeLA cell culture plates (crystal violet stained) infected with lentiviruses expressing control (LacZ) or the indicated MCM3 proteins variants. (**F**) MCM3 interacts with MCM5 via the NES motif. HeLa cells were transduced with vectors expressing MYC-tagged LacZ, $MCM3^{WT}$, $MCM3^{L4A}$ or $MCM3^{S5A}$, immunoprecipitated (right panel), and probed for MCM3, MCM5 or MCM7.

Table 1. *Mcm3* heterozygosity improves survival of $Mcm2^{IRES\text{-}CreERT2}$ homozygotes

Genotype		>3 month survival	>5 month survival
$Mcm2^{+/+}$ $Mcm3^{+/+}$		14/14	9/9
$Mcm2^{+/+}$ $Mcm3^{Gt/+}$		12/12	10/10
$Mcm2^{IRES\text{-}CreERT2/IRES\text{-}CreERT2}$	$Mcm3^{+/+}$	9/16	1/6
$Mcm2^{IRES\text{-}CreERT2/IRES\text{-}CreERT2}$	$Mcm3^{Gt/+}$	12/15	7/8*

*Significantly different from genotype above ($P = 0.0256$; Fisher's exact test).

DISCUSSION

The mechanisms of pre-RC establishment, activation and inhibition have been studied intensely. Fewer studies are how diverse cells in complex organisms modulate overall origin licensing levels. Using a genetic approach, we uncover two novel post-transcriptional phenomena that coordinate and adjust MCM levels in mice and primary cells, and relate these to *in vivo* consequences.

Most unexpected was the coordinate post-transcriptional down-regulation of Mcm mRNA in *Chaos3* cells. Two likely mechanisms are: (i) decreased mRNA stability; or (ii) active mRNA degradation. Since *Dicer1* or *Drosha* knockdown increased *Mcm2–7* mRNA levels in *Chaos3* cells, this lends support for the latter, and suggests that miRNAs are involved. We hypothesized that if this were the case, that one miRNA might bind all the *Mcm2–7* mRNAs. However, while there are numerous predicted binding sites (www.targetscan.org) for known miRNAs in the 3′-UTRs of each mRNA, no single one is predicted to

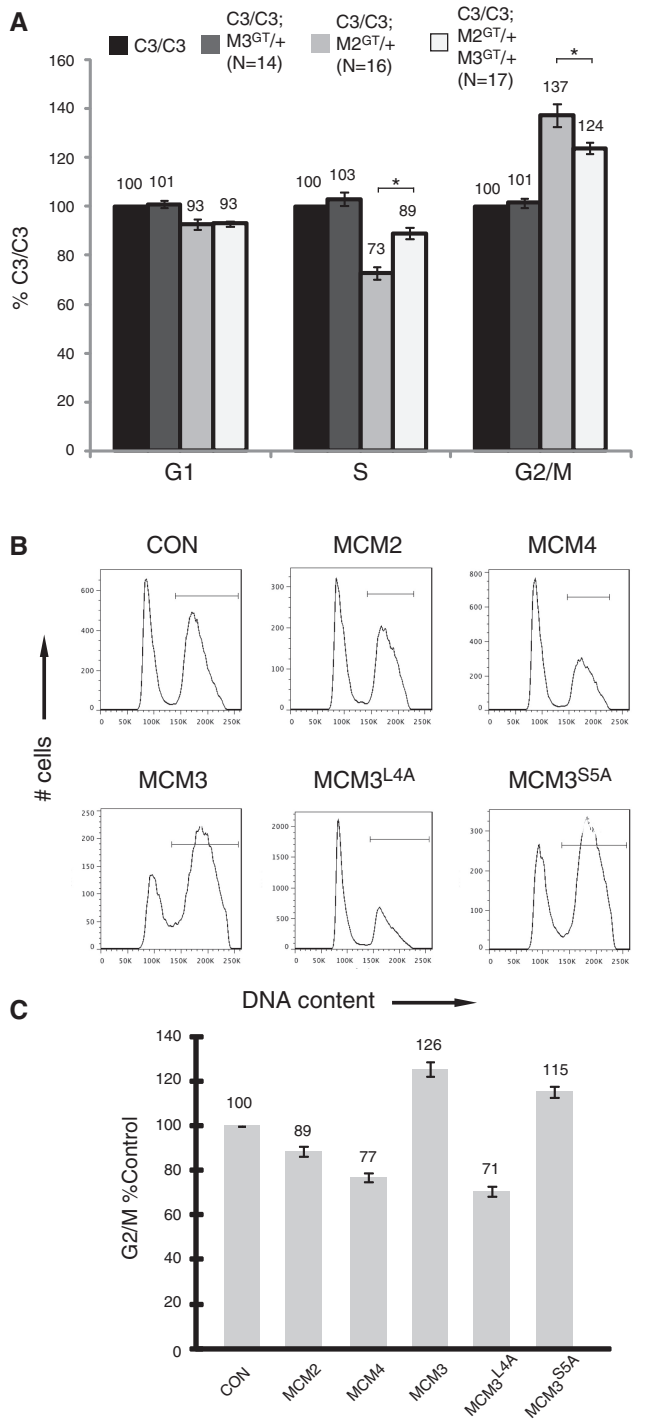

Figure 5. Defective cell cycle in MCM-deficient cells and impact of WT or mutant MCM3 levels. (**A**) Flow cytometric analysis of cell cycle in unsynchronized MEFs. The values are plotted as a percentage of the measured average of $Mcm4^{Chaos3/Chaos3}$ MEFs for each cell cycle stage (*Y*-axis), which is set to 100%. The MEFs were established from littermates. 'C3' = $Mcm4^{Chaos3}$; 'M#' = Mcm#; 'GT' is shorthand for the mutant allele of that Mcm. Error bars represent SEM, derived from at least 14 independent experiments ('*N*' numbers indicated). '*' = statistically significant to $P < 0.05$). (**B**) Cell cycle histograms of $Mcm^{C3/C3}$ $Mcm2^{+/-}$ $Mcm3^{+/-}$ MEFs infected with lentiviruses expressing the either LacZ alone ('CON') or the indicated Mcm. Only infected cells were scored, based on expression of epitope tags. (**C**) Quantification of G2/M population data (gates are shown in 'B'). The percentages of G2/M population were normalized against LacZ controls (set to 100%). Error bars represent SEM from three independent experiments.

bind all of them. This raised several alternate possibilities including: (i) the miRNA-mediated regulation is indirect; (ii) multiple miRNAs are involved; and (iii) the culprit miRNAs do not bind the 3′-UTRs.

As described earlier, recent evidence implicated involvement of the miR-34 family. miR-34a over-expression causes decreased MCM2–7 protein and RNA levels despite not having 3′-UTR seed sequences (30,31), and both *Mcm2* and *Mcm5* mRNAs were found to be associated with miR-34a in the RISC complex (31). Our finding that each of the miR-34 members are strikingly elevated in *Chaos3* MEFs is not only consistent with their being involved in the Mcm2–7 mRNA depletion phenomenon, but since miR-34b and miR-34c are more highly elevated than miR-34a in the mutant cells, the former two may play a leading role in suppressing MCM2–7 levels. Over-expression of *miR-34a-c* each decrease levels of *Mcm3* and *5* mRNAs (32). Other than the direct effects known for miR-34a upon *Mcm2* and *Mcm5*, the relationships between the 6 Mcms and the miR-34 family members remain uncertain.

Besides the actual mechanism by which Mcm mRNAs are down-regulated, a key question concerns the trigger of the mechanism. In the case of $Mcm4^{C3}$, the trigger is likely one or more of the downstream consequences of Phe345Ile mutation. These include disrupted MCM4–MCM6 interaction (Figure 3A–C), elevated DSBs and replication fork stalling that persists into G2/M and triggers DNA damage responses (11). However, the latter is hypothesized to be a consequence of reduced dormant origins (11), a condition that presumably results from the mRNA reductions demonstrated here, and therefore would be downstream of the initial trigger. While the precise trigger remains unclear, we hypothesize that TRP53 signaling is central. TRP53 directly stimulates *miR-34a-c* transcription (32), is constitutively activated in $Mcm4^{C3/C3}$ MEFs, and MCM levels increase when *Trp53* is deleted from $Mcm4^{C3/C3}$ cells (43). Although elevated TRP53 can repress Mcm transcription (44), this is not occurring in Chaos3 cells. Perhaps TRP53 is a more potent transcriptional activator of miRNA-34 than a repressor of Mcms.

Although Mcm2–7 mRNA depletion must be downstream of a trigger caused by the *Chaos3* mutation, it is possible that MCM depletion alone, if sufficient to cause replication stress, can elicit the same response. Although 50% genetic reduction of *Mcm4* or *Mcm6* in MEFs did not cause a decrease in the other Mcm mRNAs, heterozygosity for *Mcm2* did cause a minor pan-reduction ranging from 10% to 20% (10) (C.-H. Chuang, unpublished observations). Interestingly, there are reports in the literature indicative of coordinated Mcm pan-reduction mechanisms, but that the phenomena are complicated, and may vary according to organism, system and particular MCM. Numerous studies have reported MCM protein decreases in response to mutation or knockdown of a single MCM, including *Drosophila* (15) and human cells (4,13,41). In these examples of parallel MCM decreases, the general assumption is that there is hexamer destabilization or impaired loading followed by degradation of MCM monomers. This may, indeed, be true in some cases, but mRNA

levels were rarely assessed. Interestingly, an opposite regulatory phenomenon has been observed such that overexpression of certain exogenous Mcms in CHO cells caused a compensatory decreased in the corresponding endogenous protein (45). However, the basis for this was not explored.

The second post-transcriptional regulatory mechanism we found is that MCM3:MCM5 interaction blocks MCM2–7 loading onto chromatin *in vivo*, and that alteration of MCM3 levels has phenotypic consequences in parallel with the effects upon MCM loading. These results support data from *in vitro* studies that the function of this pair is regulatory in nature (21). Regarding the exact mechanism behind the inhibitory role of MCM3, we suggest that free MCM3 and/or MCM3:MCM5 decreases the amounts of their adjacent partners (MCM7 and MCM5 for MCM3; MCM2 and MCM3 for MCM5) that are available for heterohexamer formation. Supportive of this idea is a study indicating that there may be 2–3 times more MCM3 than each of the other 5 MCMs (46,47). Since $MCM3^{L4A}$ lacks negative effects on MCM2–7 loading but retains the ability to interact with MCM7, the obstructive effect would be dependent on interaction with MCM5. Our finding that MCM3 interacts with XPO1 via an NES consensus sequence raises the possibility that the MCM3:5 binding occurs in the context of nuclear pore association. However, it is unclear if nuclear export of MCM2–7 is mediated by this interaction. Interestingly, the nuclear pore complex (NPC) protein ELYS, which interacts with MCM2 and 4, is important for maintaining normal levels of dormant origins in mouse intestinal cells (48), suggesting that the NPC is an important site at which MCM licensing is governed both positively and negatively.

SUPPLEMENTARY DATA

Supplementary Data are available at NAR Online: Supplementary Table 1 and Supplementary Figure 1.

FUNDING

The National Institutes of Health (grant numbers RO1 CA130995 to S.P., P30 CA216056 to RPCI); Ellison Medical Foundation (Senior Scholar award to S.P.); Department of Defense (BC083376 to C.-H.C.); Empire State Stem Cell Fund (contract C024174 to J.S.). Funding for open access charge: Cornell Institutional funds.

Conflict of interest statement. None declared.

REFERENCES

1. Truong,L.N. and Wu,X. (2011) Prevention of DNA re-replication in eukaryotic cells. *J. Mol. Cell Biol.*, **3**, 13–22.
2. Woodward,A.M., Göhler,T., Luciani,M.G., Oehlmann,M., Ge,X., Gartner,A., Jackson,D.A. and Blow,J.J. (2006) Excess Mcm2-7 license dormant origins of replication that can be used under conditions of replicative stress. *J. Cell Biol.*, **173**, 673–683.
3. Ge,X., Jackson,D.A. and Blow,J.J. (2007) Dormant origins licensed by excess Mcm2-7 are required for human cells to survive replicative stress. *Genes Dev.*, **21**, 3331–3341.
4. Ibarra,A., Schwob,E. and Mendez,J. (2008) Excess MCM proteins protect human cells from replicative stress by licensing backup origins of replication. *Proc. Natl Acad. Sci. USA*, **105**, 8956–8961.
5. Bicknell,L.S., Bongers,E.M., Leitch,A., Brown,S., Schoots,J., Harley,M.E., Aftimos,S., Al-Aama,J.Y., Bober,M., Brown,P.A. *et al.* (2011) Mutations in the pre-replication complex cause Meier-Gorlin syndrome. *Nat. Genet.*, **43**, 356–359.
6. Bicknell,L.S., Walker,S., Klingseisen,A., Stiff,T., Leitch,A., Kerzendorfer,C., Martin,C.A., Yeyati,P., Al Sanna,N., Bober,M. *et al.* (2011) Mutations in ORC1, encoding the largest subunit of the origin recognition complex, cause microcephalic primordial dwarfism resembling Meier-Gorlin syndrome. *Nat. Genet.*, **43**, 350–355.
7. Guernsey,D.L., Matsuoka,M., Jiang,H., Evans,S., Macgillivray,C., Nightingale,M., Perry,S., Ferguson,M., LeBlanc,M., Paquette,J. *et al.* (2011) Mutations in origin recognition complex gene ORC4 cause Meier-Gorlin syndrome. *Nat. Genet.*, **43**, 360–364.
8. Shima,N., Alcaraz,A., Liachko,I., Buske,T.R., Andrews,C.A., Munroe,R.J., Hartford,S.A., Tye,B.K. and Schimenti,J.C. (2007) A viable allele of *Mcm4* causes chromosome instability and mammary adenocarcinomas in mice. *Nat. Genet.*, **39**, 93–98.
9. Pruitt,S.C., Bailey,K.J. and Freeland,A. (2007) Reduced *Mcm2* expression results in severe stem/progenitor cell deficiency and cancer. *Stem Cells*, **25**, 3121–3132.
10. Chuang,C.H., Wallace,M.D., Abratte,C., Southard,T. and Schimenti,J.C. (2010) Incremental genetic perturbations to MCM2-7 expression and subcellular distribution reveal exquisite sensitivity of mice to DNA replication stress. *PLoS Genet.*, **6**, e1001110.
11. Kawabata,T., Luebben,S.W., Yamaguchi,S., Ilves,I., Matise,I., Buske,T., Botchan,M.R. and Shima,N. (2011) Stalled fork rescue via dormant replication origins in unchallenged S phase promotes proper chromosome segregation and tumor suppression. *Mol. Cell*, **41**, 543–553.
12. Tsao,C.C., Geisen,C. and Abraham,R.T. (2004) Interaction between human MCM7 and RAD17 proteins is required for replication checkpoint signaling. *EMBO J.*, **23**, 4660–4669.
13. Cortez,D., Glick,G. and Elledge,S.J. (2004) Minichromosome maintenance proteins are direct targets of the ATM and ATR checkpoint kinases. *Proc. Natl Acad. Sci. USA*, **101**, 10078–10083.
14. Orr,S.J., Gaymes,T., Ladon,D., Chronis,C., Czepulkowski,B., Wang,R., Mufti,G.J., Marcotte,E.M. and Thomas,N.S. (2010) Reducing MCM levels in human primary T cells during the G(0) → G(1) transition causes genomic instability during the first cell cycle. *Oncogene*, **29**, 3803–3814.
15. Crevel,G., Hashimoto,R., Vass,S., Sherkow,J., Yamaguchi,M., Heck,M.M. and Cotterill,S. (2007) Differential requirements for MCM proteins in DNA replication in Drosophila S2 cells. *PLoS One*, **2**, e833.
16. Buchsbaum,S., Morris,C., Bochard,V. and Jalinot,P. (2007) Human INT6 interacts with MCM7 and regulates its stability during S phase of the cell cycle. *Oncogene*, **26**, 5132–5144.
17. Bochman,M.L. and Schwacha,A. (2009) The Mcm complex: unwinding the mechanism of a replicative helicase. *Microbiol. Mol. Biol. Rev.*, **73**, 652–683.
18. Ishimi,Y. (1997) A DNA helicase activity is associated with an MCM4, -6, and -7 protein complex. *J. Biol. Chem.*, **272**, 24508–24513.
19. Lee,J.K. and Hurwitz,J. (2001) Processive DNA helicase activity of the minichromosome maintenance proteins 4, 6, and 7 complex requires forked DNA structures. *Proc. Natl Acad. Sci. USA*, **98**, 54–59.
20. Ishimi,Y., Ichinose,S., Omori,A., Sato,K. and Kimura,H. (1996) Binding of human minichromosome maintenance proteins with histone H3. *J. Biol. Chem.*, **271**, 24115–24122.
21. Schwacha,A. and Bell,S.P. (2001) Interactions between two catalytically distinct MCM subgroups are essential for coordinated ATP hydrolysis and DNA replication. *Mol. Cell.*, **8**, 1093–1104.
22. Sato,M., Gotow,T., You,Z., Komamura-Kohno,Y., Uchiyama,Y., Yabuta,N., Nojima,H. and Ishimi,Y. (2000) Electron microscopic observation and single-stranded DNA binding activity of the Mcm4,6,7 complex. *J. Mol. Biol.*, **300**, 421–431.

23. Brambrink,T., Foreman,R., Welstead,G.G., Lengner,C.J., Wernig,M., Suh,H. and Jaenisch,R. (2008) Sequential expression of pluripotency markers during direct reprogramming of mouse somatic cells. *Cell Stem Cell*, **2**, 151–159.
24. Frisa,P.S. and Jacobberger,J.W. (2010) Cytometry of chromatin bound Mcm6 and PCNA identifies two states in G1 that are separated functionally by the G1 restriction point. *BMC Cell Biol.*, **11**, 26.
25. Friedrich,T.D., Bedner,E., Darzynkiewicz,Z. and Lehman,J.M. (2005) Distinct patterns of MCM protein binding in nuclei of S phase and rereplicating SV40-infected monkey kidney cells. *Cytometry A*, **68**, 10–18.
26. Reinholdt,L., Ashley,T., Schimenti,J. and Shima,N. (2004) Forward genetic screens for meiotic and mitotic recombination-defective mutants in mice. *Methods Mol. Biol.*, **262**, 87–107.
27. Elferink,C.J. and Reiners,J.J. Jr (1996) Quantitative RT-PCR on CYP1A1 heterogeneous nuclear RNA: a surrogate for the in vitro transcription run-on assay. *Biotechniques*, **20**, 470–477.
28. Sugimoto,K., Mori,K., Uchida,K., Kobayashi,D. and Itoi,K. (2007) Quantitative analysis of thyroid-stimulating hormone messenger RNA and heterogeneous nuclear RNA in hypothyroid rats. *Brain Res. Bull.*, **74**, 142–146.
29. Kuehbacher,A., Urbich,C., Zeiher,A.M. and Dimmeler,S. (2007) Role of Dicer and Drosha for endothelial microRNA expression and angiogenesis. *Circ. Res.*, **101**, 59–68.
30. Kaller,M., Liffers,S.T., Oeljeklaus,S., Kuhlmann,K., Röh,S., Hoffmann,R., Warscheid,B. and Hermeking,H. (2011) Genome-wide characterization of miR-34a induced changes in protein and mRNA expression by a combined pulsed SILAC and microarray analysis. *Mol. Cell. Proteomics*, **10**, M111.010462.
31. Lal,A., Thomas,M.P., Altschuler,G., Navarro,F., O'Day,E., Li,X.L., Concepcion,C., Han,Y.C., Thiery,J., Rajani,D.K. *et al.* (2011) Capture of MicroRNA-Bound mRNAs Identifies the Tumor Suppressor miR-34a as a Regulator of Growth Factor Signaling. *PLoS Genet.*, **7**, e1002363.
32. He,L., He,X., Lim,L.P., de Stanchina,S.E., Xuan,Z., Liang,Y., Xue,W., Zender,L., Magnus,J., Ridzon,D. *et al.* (2007) A microRNA component of the p53 tumour suppressor network. *Nature*, **447**, 1130–1134.
33. Yamakuchi,M., Lotterman,C.D., Bao,C., Hruban,R.H., Karim,B., Mendell,J.T., Huso,D. and Lowenstein,C.J. (2010) P53-induced microRNA-107 inhibits HIF-1 and tumor angiogenesis. *Proc. Natl Acad. Sci. USA*, **107**, 6334–6339.
34. Li,X., Schimenti,J. and Tye,B. (2009) Aneuploidy and improved growth are coincident but not causal in a yeast cancer model. *PLoS Biol.*, **7**, e1000161.
35. Remus,D., Beuron,F., Tolun,G., Griffith,J.D., Morris,E.P. and Diffley,J.F. (2009) Concerted loading of Mcm2-7 double hexamers around DNA during DNA replication origin licensing. *Cell*, **139**, 719–730.
36. Kunnev,D., Rusiniak,M.E., Kudla,A., Freeland,A., Cady,G.K. and Pruitt,S.C. (2010) DNA damage response and tumorigenesis in *Mcm2*-deficient mice. *Oncogene*, **29**, 3630–3638.
37. Liku,M.E., Nguyen,V.Q., Rosales,A.W., Irie,K. and Li,J.J. (2005) CDK phosphorylation of a novel NLS-NES module distributed between two subunits of the Mcm2-7 complex prevents chromosomal rereplication. *Mol. Biol. Cell*, **16**, 5026–5039.
38. Madine,M.A., Khoo,C.Y., Mills,A.D., Musahl,C. and Laskey,R.A. (1995) The nuclear envelope prevents reinitiation of replication by regulating the binding of MCM3 to chromatin in Xenopus egg extracts. *Curr. Biol.*, **5**, 1270–1279.
39. Gillespie,P.J., Khoudoli,G.A., Stewart,G., Swedlow,J.R. and Blow,J.J. (2007) ELYS/MEL-28 chromatin association coordinates nuclear pore complex assembly and replication licensing. *Curr. Biol.*, **17**, 1657–1662.
40. Ishimi,Y., Okayasu,I., Kato,C., Kwon,H.J., Kimura,H., Yamada,K. and Song,S.Y. (2003) Enhanced expression of Mcm proteins in cancer cells derived from uterine cervix. *Eur. J. Biochem.*, **270**, 1089–1101.
41. Lin,D.I., Aggarwal,P. and Diehl,J.A. (2008) Phosphorylation of MCM3 on Ser-112 regulates its incorporation into the MCM2-7 complex. *Proc. Natl Acad. Sci. USA*, **105**, 8079–8084.
42. Burkhart,R., Schulte,D., Hu,D., Musahl,C., Göhring,F. and Knippers,R. (1995) Interactions of human nuclear proteins P1Mcm3 and P1Cdc46. *Eur. J. Biochem.*, **228**, 431–438.
43. Kawabata,T., Yamaguchi,S., Buske,T., Luebben,S.W., Wallace,M., Matise,I., Schimenti,J.C. and Shima,N. (2011) A reduction of licensed origins reveals strain-specific replication dynamics in mice. *Mamm. Genome*, **22**, 506–517.
44. Scian,M.J., Carchman,E.H., Mohanraj,L., Stagliano,K.E., Anderson,M.A., Deb,D., Crane,B.M., Kiyono,T., Windle,B., Deb,S.P. *et al.* (2008) Wild-type p53 and p73 negatively regulate expression of proliferation related genes. *Oncogene*, **27**, 2583–2593.
45. Kuipers,M., Stasevich,T., Sasaki,T., Wilson,K., Hazelwood,K., McNally,J., Davidson,M. and Gilbert,D. (2011) Highly stable loading of Mcm proteins onto chromatin in living cells requires replication to unload. *J. Cell Biol.*, **192**, 29–41.
46. Wong,P.G., Winter,S.L., Zaika,E., Cao,T.V., Oguz,U., Koomen,J.M., Hamlin,J.L. and Alexandrow,M.G. (2011) Cdc45 limits replicon usage from a low density of preRCs in mammalian cells. *PLoS One*, **6**, e17533.
47. Schulte,D., Burkhart,R., Musahl,C., Hu,B., Schlatterer,C., Hameister,H. and Knippers,R. (1995) Expression, phosphorylation and nuclear localization of the human P1 protein, a homologue of the yeast Mcm 3 replication protein. *J. Cell Sci.*, **108(Pt 4)**, 1381–1389.
48. Gao,N., Davuluri,G., Gong,W., Seiler,C., Lorent,K., Furth,E.E., Kaestner,K.H. and Pack,M. (2011) The nuclear pore complex protein Elys is required for genome stability in mouse intestinal epithelial progenitor cells. *Gastroenterology*, **140**, 1547–1555.